Determining the Arrangement and Cooperative Operating Control of Two Industrial Robots During Wire Driving Tasks Considering Torque Margin and Manipulability Characteristics

Akihiro Nabeshima*, Toshiki Hirogaki, and Eiichi Aoyama

Abstract—When multiple robots perform a task, the user generally arranges the robots based on their working range. However, this criterion alone may place an unnecessarily large load on a robot joints. On the other hand, developments in IoT technology have facilitated the acquisition of servo information from robots and other devices. This information is expected to become increasingly important in the future. In this study, two small multi-joint robots are used to propose a method to determine robot placement based on criteria different from the robot working range. The proposed method is constructed by focusing on the joint torque working on the robot, which can be easily obtained using IoT technology. In addition, focusing on the torque margin and operating force ellipsoid derived from manipulability, we examine the cooperation of two robots to lift a weight that exceeds the range of motion of a single robot exerting a constant external force.

Index Terms—Industrial robot, torque margin, determining the arrangement

I. Introduction

The importance of factory automata (FA) technology is increasing to maintain the international competitiveness of the Japanese manufacturing industry [1]. The basis for the FA technique commonly uses a combination of industrial robots, CNC machine tools, and automatic guided vehicles (AGVs). To realize a flexible FA system, the need for a provision of turning motor function, similar to industrial robots, has been increasing for machine tools with 5-axis control for schemes that control the movement of the two-axis rotations in three-axis translations in recent years. Subsequently, such machining centers have been put into practical use and become widely adopted. On the other hand, the motion control of the column or table is based on the guide structure and position of the pivot shaft center that is fixed to the structure. Therefore, machining centers have been greatly limited regarding how freely they can operate during turning operations [2]. A machining center has no guide structure, a parallel mechanism system that supports a table by combining spherical joints with other degrees of freedom, and the ball screw guide has been used in practice. Despite some precision calibration and size of the machine, owing to the interference of the joint problems uncertainties are obvious [3]. However, the degree of freedom of a workstation required large movements by the multi-joint robots, which are not suitable fortion. Subsequently, maintains a low support stiffness is maintained on the table to carry out the machining process on the table. However, the synchronous polyaxial control technique has been implemented owing to the developments in CNC technology in recent years. For example, double-bowl robot configured as a one-armed articulated robot arm has been adopted in practice, and applications of new FA techniques are expected.

Path planning while gripping flexible objects and performing obstacle avoidance is a recent research topic regarding dual-arm robots [4]. Furthermore, there is an evaluation method that analyzes the trajectory rolling motion of the ball on the plate that supports the work plate. The DBB method for evaluating the motion accuracy of the simultaneous two-axis control is another common approach [5]. However, the articulated robot currently used is large and expensive, whose operation is spot-like considering that the operation used two or more sets. Therefore, in the previous reports [6, 7], focusing on the joint torque of the robot, we determined the arrangement to reduce the output torque by considering the various arrangements of two compact and relatively inexpensive articulated robots. However, an index focusing only on the torque margin may be inappropriate from a motion accuracy standpoint; subsequently, we attempted to propose an improved placement determination method by using an index that considers the operating force ellipsoid derived from manipulability. Therefore, we examine the index by focusing on the torque margin and operating force ellipsoid and consider the lifting a given payload under a constant external force.

II. Experimental Device and Theory

A. Experimental Device

The Academic Robot VE-026A (Fig. 1) made by Denso Wave was employed. This robot has a 7-axis structure with a 6-axis arm and 1-axis hand and can mimic the movement a human arm. The robot weighs 355 g, and is 278 mm long

when fully extended; thus, the robot is compact and lightweight. In this study, we employed two of these robots and attempted to realize a cooperative operation on a two-dimensional plane using three motors.
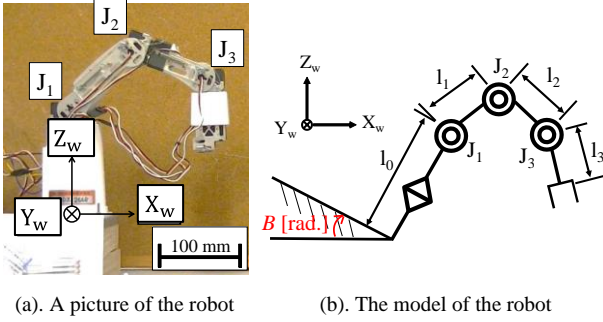

(a). A picture of the robot (b). The model of the robot

Fig. 1. The robot made by DENSO WAVE(VEO026A).

B. Basic Theory (Torque Margin)

The end effector outputs were F_{ex} and F_{ez}, and the torque required for each joint was τ_1, τ_2, and τ_3. The relationships among these parameters are defined in the following equations. Let the links of the robot arm be defined as links 0, 1, 2, and 3, joints be defined as J_1, J_2, and J_3, and lengths of the links be l0, l1, l2, and l3. Furthermore, let the motion angles of each joint be θ_1, θ_2, and θ_3, respectively. In this study, we do not output the rotation on the XZ plane to the end-effector. Here, X and Z axes are horizontal and vertical, respectively. Therefore,

$$\tau_1 = J_{11}F_{ex} + J_{21}F_{ez} \quad (1)$$

$$\tau_2 = J_{12}F_{ex} + J_{22}F_{ez} \quad (2)$$

$$\tau_3 = J_{13}F_{ex} + J_{23}F_{ez} \quad (3)$$

J_{ij} (i，j = 1，2，and 3) indicates each element of the robot Jacobian matrix.

However, the abovementioned equations do not consider the weight of the robot and only indicate the relationship between the external force acting on a simple end effector and load torque acting on each joint. Because the weight of an actual robot acts on itself as well, we consider the influence of the robot arm weight as shown in Fig. 2.
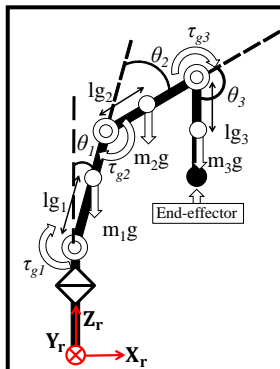

Fig. 2. Torque value influenced by the robot weight.

l_{g1}, l_{g2}, and l_{g3} denote the center of gravity positions of each link, and m_1, m_2, and m_3 denote the weights of each link. Assuming that the gravitational acceleration is g, the true

output torques τ_{s1}, τ_{s2}, and τ_{s3} required at each joint can be obtained as follows.

$$\tau_{s1} = \tau_1 - [m_1 g l_{g1} sin\theta_1 + m_2 g\{l_1 sin\theta_1 + l_{g2} sin(\theta_1 + \theta_2)\} + m_3 g\{(l_1 sin\theta_1 + l_2 sin(\theta_1 + \theta_2) + l_{g3} sin(\theta_1 + \theta_2 + \theta_3)\}] \quad (4)$$

$$\tau_{s2} = \tau_2 - [m_2 g l_{g2} sin(\theta_1 + \theta_2) + m_3 g\{l_2 sin(\theta_1 + \theta_2) + l_{g3} sin(\theta_1 + \theta_2 + \theta_3)\}] \quad (5)$$

$$\tau_{s3} = \tau_3 - \{m_3 g l_{g3} sin(\theta_1 + \theta_2 + \theta_3)\} \quad (6)$$

We define a numerical value N_τ to evaluate the margin of the joint torque for the robot. Consider the value obtained by subtracting the required torque τ_{si} (i = 1, 2, 3) from the maximum torque τ_{iMAX} (i = 1, 2, 3), where the servo motor can output the output margin. This value is defined as τ_{ai} (i = 1, 2, 3) as follows.

$$\tau_{ai} = \tau_{iMAX} - |\tau_{si}| \quad (7)$$

Furthermore, the second-order norm $\|N_\tau\|_2$ is given as:

$$\|N_\tau\|_2 = \sqrt{|\tau_{a1}|^2 + |\tau_{a2}|^2 + |\tau_{a3}|^2} \quad (8)$$

Note that when one τ_{ai} is negative, there is no margin, which corresponds to an inoperable state; thus, resulting in $N_\tau = 0$. Furthermore, the maximum value of N_τ is $N_{\tau MAX}$, and the second-order norm $\|N_{\tau MAX}\|_2$ is

$$\|N_{\tau MAX}\|_2 = \sqrt{|\tau_{1MAX}|^2 + |\tau_{2MAX}|^2 + |\tau_{3MAX}|^2} \quad (9)$$

From Eqs. (14) and (15), the torque margin $N_{\tau P}$, which is used to evaluate the joint torque margin of the entire robot, can be defined as follows.

$$N_{\tau P} = \|N_\tau\|_2 / \|N_{\tau MAX}\|_2 \times 100 \quad (10)$$

$N_{\tau P}$ is an index that indicates the margin of the entire joint. The higher the value of $N_{\tau P}$ is, the better the configuration is.

III. EXPERIMENTAL METHODS

A. Experimental Conditions and Methods

In this section, the procedure for determining the placement of the two robots is described. The model of the apparatus used in this study is presented in Fig. 3. The robot on the left is defined as the sub-arm, and the robot on the right is defined as the main arm. The payload weight is 0.49 N. The target motion of the experiment was to move the payload only in the Z_w axis direction and not in the X_w axis direction. After both arms were moved to their initial states, the heights of the two robot bases were changed, and the tegus between the end-effectors were leveled. The end-effector of the sub-arm was moved by 50 mm in the Z_w direction and −50 mm in the X_w direction. The end-effector of the main arm was moved by 50 mm in the Z_w direction to maintain a constant external force at a distance of 100 mm. The ground plane angle was set to Π/2 rad. for the main arm and −Π/4 rad. for the sub-arm,

which were described as optimal values in previous studies. The experiment was conducted with an operating time of 1 s.

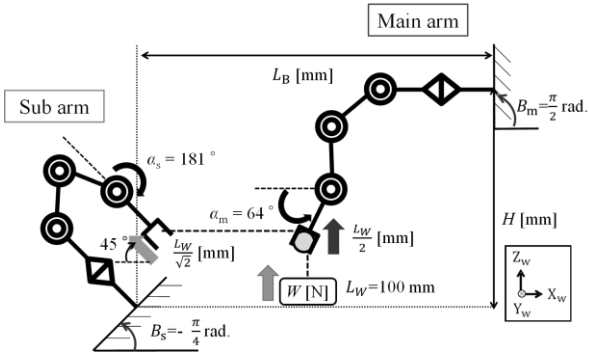Fig. 3. Model of the experimental device.

B. Definition of Operating Error

Fig. 4 illustrates the positional relationship between the trajectory in the actual operation and theoretical trajectory. If the theoretical error along the orbit axis is Δsk [mm], vertical error is Δtk [mm], and total number of plots is c, the error ε [mm] per plot is given by Eq. (11).
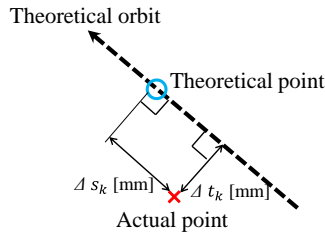

Fig. 4. The positional relationship.

$$\varepsilon = \frac{\sum_{k=1}^{c}(\Delta s_k + \Delta t_k)}{c} \qquad (11)$$

IV. DEFINITION OF THE OPERATING FORCE TORQUE MARGIN

A. Calculating the Operating Force Ellipsoid

The operating force ellipsoid is more likely to exert a force in the long-axis direction and less likely to exert a force in the short-axis direction. In this study, we examined an index that considers the properties of an operating-force ellipsoid. The operating force ellipsoid is a set of all f [N] that can be realized using a joint torque τ [N・m] that satisfies Eq. (13), which is based on the relationship between the joint torque τ [N・m] and force f [N] applied to the object stated in Eq. (12).

$$\tau = J^T f \qquad (12)$$

$$\|\tau\| = (\tau^T \tau)^{\frac{1}{2}} \leq 1 \qquad (13)$$

The singular value decomposition of the Jacobian matrix J is given by Eq. (14). Matrices U and V are m × m and n × n orthogonal matrices, respectively. Σ is represented by Eq. (15). $\sigma_1, \sigma_2, …, \sigma_m$ are the singular values of J and are the square roots of eigenvalues λ_i ($i = 1, …, m$) of the matrix JJ^T in an increasing order. The principal axes of the operational force ellipsoid are given by $u_1/\sigma_1, u_2/\sigma_2, …, u_i/\sigma_i$, if the

column i vector of matrix U is denoted by u_i.

$$J = U\Sigma V^T \qquad (14)$$

$$\Sigma = \begin{bmatrix} \sigma_1 & \cdots & 0 \\ \vdots & \ddots & \vdots \\ 0 & \cdots & \sigma_m \end{bmatrix} \qquad (15)$$

$$\sigma_1 \geq \sigma_2 \geq \cdots \geq \sigma_m \geq 0 \qquad (16)$$

B. Definition of the Operating Force Torque Margin

Fig. 5 presents an operating force ellipsoid that indicates in which direction the end-effector tends to exert a force. In Fig. 5, L1 [mm] denotes the diameter of the major axis of the ellipsoid, L2 [mm] denotes the diameter of the minor axis, and θ [rad.] denotes the angle between the direction of motion and major axis of the ellipsoid. Assuming that the end-effector is at the center of this operating force ellipsoid, it is more likely to exert a force in the direction of the long axis of the operating force ellipsoid and less likely to exert a force in the direction of the short axis. The index of the torque margin plus the operating force ellipsoid and direction of motion is defined as the operating force torque margin, as stated in Eq. (17). The operating force torque margin is calculated to be small when the end-effector moves in the direction of the short axis of the operable ellipsoid or when the short-axis diameter of the ellipsoid is extremely small compared to the long-axis diameter. Therefore, we believe that the operation force torque margin can be used to determine a better arrangement, not only in terms of the load on each joint but also in terms of motion accuracy.

$$N_{\tau Pf} = \frac{\|N_\tau\|_2}{\|N_{\tau Max}\|_2} \times \frac{L_2}{L_1} \times \cos\theta \times 10^6 \qquad (17)$$
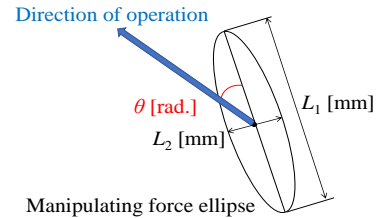

Fig. 5. Manipulating the force ellipse.

Fig. 6 shows the positional relationship between the operating force torque margin defined by Eq. (17) and end-effector. Orbits ① to ⑤ in the figure exhibit lower operating force torque margins. Experiments were conducted in orbits ① to ⑤, and the relationship between the index, power consumption, and operating error was discussed.
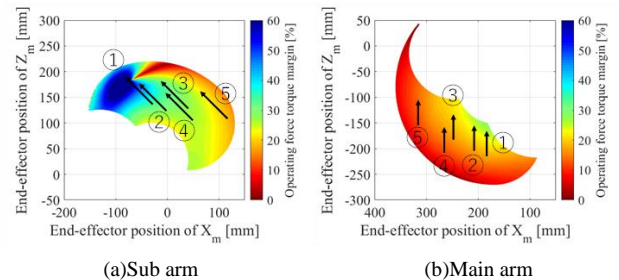

(a)Sub arm (b)Main arm

Fig. 6. Operating force torque margin diagrams.

V. Experimental Results and Discussion

A. Operating Force Torque Margin and Power Consumption

Fig. 7 depicts the power consumption graphs for both arms, and Fig. 8 shows the total power consumption for each trajectory. These figures indicate that as the operating force torque margin increases and an optimum trajectory is achieved, the load on the joints is reduced and power consumption is reduced. This means that the operating force torque margin can be used to determine the placement and trajectory that minimizes the load on the joints and power consumption.
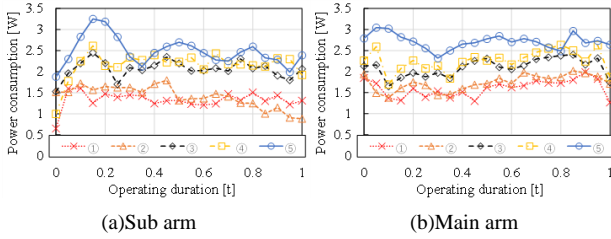

(a)Sub arm   (b)Main arm
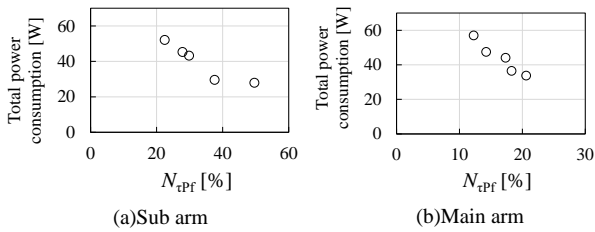Fig. 7. Power consumptions.

(a)Sub arm   (b)Main arm
Fig. 8. Total power consumptions.

B. Operating Force Torque Margin and Motion Error

Fig. 9 shows the relationship between the torque margin and operating error, which is the conventional index. This figure shows that, in the main arm, the operating error increases as the torque margin increases when the trajectory is considered optimal. Fig. 10 shows the relationship between the operating force torque margin and operating error proposed in this study. These figures show that, except for the trajectory with the highest operating force torque margin (trajectory ①), the operating error decreases as the operating force torque margin increases. In orbit 1, the power consumption of the second joint was extremely high compared with that of the other joints, which may have increased the motion error. Therefore, in practice, it is necessary to incorporate a factor that avoids concentrating the load on a single joint into the index. These results indicate that the operating force torque margin can be used to determine the placement and trajectory with the smallest operating error.
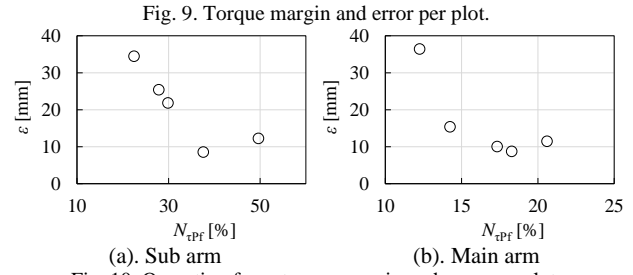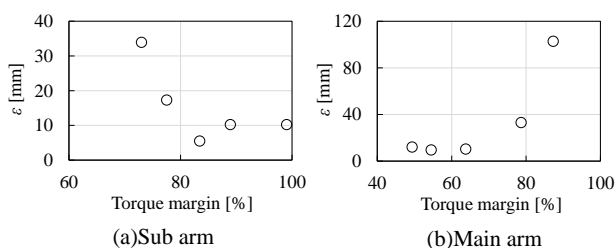

(a)Sub arm   (b)Main arm

Fig. 9. Torque margin and error per plot.

(a). Sub arm   (b). Main arm
Fig. 10. Operating force torque margin and error per plot.

VI. Conclusion

In this study, using two compact and relatively inexpensive multi-joint robots, we proposed a method for determining the trajectory and arrangement that can reduce the load on the joints, conserve power, and operate with minimal motion error by using an index that considers the torque output of each robot joint and operating force ellipsoid derived from manipulability. The following results were obtained:

- By using the operating force torque margin, it is possible to determine the placement and trajectory with a low power consumption and small operating error.
- To determine a more realistic index, it is necessary to incorporate a factor that avoids concentrating the load on a single joint.

Conflict of Interest
The authors declare no conflict of interest.

Author Contributions

Professor Hirogaki and Professor Aoyama taught me how to organize data and how to make observations. They also taught me how to correct and write my research.

References

[1] R. Y. Zhong, L. Wang, and X. Xu, "An IoT-enabled realtime machine status monitoring approach for cloud manufacturing," *Procedia CIRP*, vol. 63, pp. 709–714, 2017.
[2] T. Shibukawa, T. Taizo, and K. Hattori, "Parallel mechanism based milling machine," *Journal of the Japan Society for Precision Engineering*, vol. 63, no. 12, pp. 1671–1675, 1997.
[3] T. Matsushita, O. Tadahiro, and A. Mori, "The accuracy of cone frustum machined by five-axis machine tool with tilting table," *Journal of the Japan Society for Precision Engineering*, vol. 74, no. 6, pp. 632–636, 2008.
[4] T. Hirano, M. Yamamoto, and A. Mori, "Cooperative motion planning of two manipulators for concave wall tracing task," *Transactions of the Japan Society of Mechanical Engineers, Series C*, vol. 78, no.793, pp. 3317–3330, 2012.
[5] W. Wu, T. Hirogaki, and E. Aoyama, "Controlling a working plate with new industrial Dual-Arm robots," in *Proc. International Symposium on Flexible Automation 2010 JPS2497*, pp. 1–4, 2010.
[6] T. Sugiura, T. Hirogaki, and E. Aoyama, "Novel arrangement method of two industrial robots based on monitoring motor electric current," in *Proc. 8th International Conference on Leading Edge Manufacturing in 21st Century (LEM21),* no. 0402, pp.1–5, 2015.
[7] T. Kadoya, T. Hirogaki, and E. Aoyama, "Operating control method of two industrial robots based on monitoring motor electric current," in *Proc. International Conference of Asian Society for Precision Engneering and Nanotechnology ASPEN2017*, ARM-O-02, pp. 1–5, 2017.